Chemical Science

ROYAL SOCIETY OF CHEMISTRY

EDGE ARTICLE

View Article Online
View Journal | View Issue

Cite this: *Chem. Sci.*, 2023, **14**, 9795

All publication charges for this article have been paid for by the Royal Society of Chemistry

Gas-phase preparation of azulene ($C_{10}H_8$) and naphthalene ($C_{10}H_8$) *via* the reaction of the resonantly stabilized fulvenallenyl ($C_7H_5^\bullet$) and propargyl ($C_3H_3^\bullet$) radicals†

Wang Li,[a] Jiuzhong Yang,[a] Long Zhao,*[ab] David Couch,[c] Myrsini San Marchi,[c] Nils Hansen,*[c] Alexander N. Morozov,[d] Alexander M. Mebel*[d] and Ralf I. Kaiser*[e]

Synthetic routes to the 10π Hückel aromatic azulene ($C_{10}H_8$) molecule, the simplest polycyclic aromatic hydrocarbon carrying an adjacent five- and seven-membered ring, have been of fundamental importance due to the role of azulene – a structural isomer of naphthalene – as an essential molecular building block of saddle-shaped carbonaceous nanostructures such as curved nanographenes and nanoribbons. Here, we report on the very first gas phase preparation of azulene by probing the gas-phase reaction between two resonantly stabilized radicals, fulvenallenyl ($C_7H_5^\bullet$) and propargyl ($C_3H_3^\bullet$), in a molecular beam through isomer-resolved vacuum ultraviolet photoionization mass spectrometry. Augmented by electronic structure calculations, the novel Fulvenallenyl Addition Cyclization Aromatization (FACA) reaction mechanism affords a versatile concept for introducing the azulene moiety into polycyclic aromatic systems thus facilitating an understanding of barrierless molecular mass growth processes of saddle-shaped aromatics and eventually carbonaceous nanoparticles (soot, interstellar grains) in our universe.

Received 25th June 2023
Accepted 23rd August 2023

DOI: 10.1039/d3sc03231k

rsc.li/chemical-science

Introduction

Since the very first synthesis of the non-alternant 10π-Hückel aromatic azulene molecule ($C_{10}H_8$) by Pfau and Plattner in 1939 from octahydronaphthalene (Scheme 1),[1] five-, six-, and seven-membered organic ring moieties have emerged as fundamental molecular building blocks in 2-dimensional (graphenes, nanoflakes),[2–5] 3-dimensional (nano bowls, nanotubes, fullerenes),[3,6–11] and saddle-shaped[12] polycyclic aromatic hydrocarbons (PAHs) (Scheme 2). These carbon-based nanostructures are of fundamental significance in the fields of material science, physical (organic) chemistry and astrophysics. This is due to their exceptional photophysical properties from the narrow highest occupied molecular orbital (HOMO) – lowest unoccupied molecular orbital (LUMO) energy gaps[13] and resonance delocalization,[14] exploitation as organic field-effect transistors (OFETs),[15,16] organic conductors,[17] and non-linear optical materials,[18] as well as potential carriers of selected diffuse interstellar bands (DIBs)[19,20] – discrete absorption features overlaid on the interstellar extinction curve covering the blue visible (400 nm) to the near-infrared (1.2 mm) region. Aromatic structures also serve as precursors to carbonaceous nanoparticles in combustion systems ('soot particles')[21] and in circumstellar envelopes of carbon-rich Asymptotic Giant Branch (AGB) stars[22–24] along with planetary nebulae as their descendants ('circumstellar grains').[22,25–27] Whereas a mechanistical framework of the formation of PAHs carrying five- and six-membered ring moieties is beginning to emerge,[28] the gas-phase synthetic routes to polycyclic aromatic hydrocarbons incorporating seven membered rings, in particular those carrying azulene building blocks in which a five membered ring is annulated to a seven membered ring, are still elusive.[15,29]

Classical preparative organic synthesis to azulene derivatives exploit, *e.g.*, active methylene reagents *via* Nozoe's method,[30,31]

[a]*National Synchrotron Radiation Laboratory, University of Science and Technology of China, Hefei, Anhui 230029, China. E-mail: zhaolong@ustc.edu.cn*

[b]*School of Nuclear Science and Technology, University of Science and Technology of China, Hefei, Anhui 230027, China*

[c]*Combustion Research Facility, Sandia National Laboratories, Livermore, CA 94551, USA. E-mail: nhansen@sandia.gov*

[d]*Department of Chemistry and Biochemistry, Florida International University, Miami, FL 33199, USA. E-mail: mebel@fiu.edu*

[e]*Department of Chemistry, University of Hawaii at Manoa, Honolulu, HI 96822, USA. E-mail: ralfk@hawaii.edu*

† Electronic supplementary information (ESI) available: Experimental section (Fig. S1–S3); additional PIE curves (Fig. S4–S8); phthalide pyrolysis (Fig. S9–S11); absolute photoionization cross-section (PICS) of azulene (Fig. S12); fit of PIE at m/z = 128 (Fig. S13–S14); computational methods (Section 6); potential energy diagram illustrated with the structures of representative transition states (Fig. S15); product branching ratios (Fig. S16). See DOI: https://doi.org/10.1039/d3sc03231k

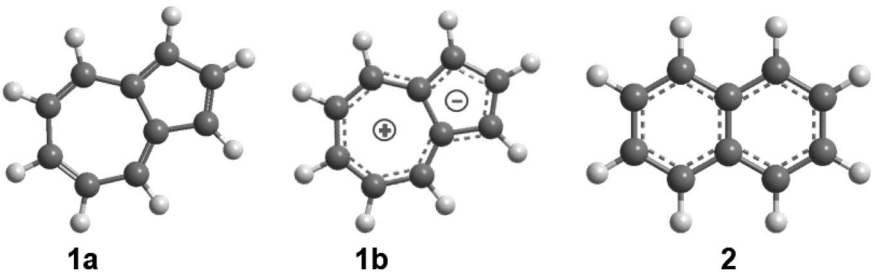

Scheme 1 Molecular structures of the azulene (**1a** and **1b**) and naphthalene (**2**) isomers ($C_{10}H_8$); atoms are color coded in gray (carbon) and white (hydrogen).

Scholl-type oxidative cyclization[32] and Aldol condensations coupled with Vilsmeier–Hack reactions and Suzuki coupling[33] effectively incorporating azulenes into helical nanographenes with twisting angles exceeding 16° (ref. 32 and 34) and non-planar acenes moieties isoelectronic to pentacene ($C_{22}H_{14}$), hexacene ($C_{26}H_{16}$) and heptacene ($C_{30}H_{18}$).[32] Seven-membered rings were also incorporated into polycyclic molecules *via* palladium-catalyzed intramolecular arylation efficiently yielding C_3-symmetric propeller shaped PAHs bearing three seven-membered rings and three [4]helicene units.[35] Würthner *et al.* established an elegant synthetic protocol for preparing saddle-shaped corannulene derivatives bearing both a positive and negative curvature at the corannulene and annulated seven-membered ring moieties.[36] Nevertheless, regardless of these astonishing advances on the preparative synthesis and characterization of azulene derivatives, gas-phase molecular mass growth processes to azulene – the simplest representative of a bicyclic, 10π aromatic molecule formally accessed through fusion of cyclopentadiene and cycloheptatriene rings – along with its derivatives in high-temperature combustion systems and extraterrestrial settings have not been reported yet, but are fundamental to unravel the gas phase preparation of carbonaceous nanostructures such as curved nanographenes[37,38] and nanoribbons.[39]

Here, we provide persuasive testimony on the first gas phase preparation of the azulene molecule ($C_{10}H_8$) along with its naphthalene isomer ($C_{10}H_8$) initiated through the reaction of two resonantly stabilized free radicals – fulvenallenyl ($C_7H_5^\bullet$) and propargyl ($C_3H_3^\bullet$) – *via* de-factor ring annulation within a chemical microreactor[40–42] *via* the novel Fulvenallenyl Addition Cyclization Aromatization (FACA) reaction mechanism. The reaction products were sampled in a molecular beam *via* electron ionization[43–45] and isomer-specifically *via* fragment-free photoionization of the neutral products exploiting tunable vacuum ultraviolet (VUV) light followed by detection of the ionized molecules in a reflection time-of-flight mass spectrometer[41,46] (Re-TOF-MS; Fig. S1 and S2, ESI†). Augmented by electronic structure calculations, the unexpected gas phase preparation of azulene from the bottom-up serves as an unconventional entry point to curved aromatics in combustion systems[21,47] and in carbon-rich, circumstellar environments.[48–50] The fulvenallenyl ($C_7H_5^\bullet$) radical can be generated from fulvenallene (C_7H_6)[51,52] through hydrogen abstraction at elevated temperatures above 1000 K as in combustion flames and in circumstellar envelopes close to the central star or *via* photolysis of the C–H bond by the internal ultraviolet field existing even deep inside molecular clouds such as the Taurus Molecular Cloud-1 (TMC-1), where fulvenallene (C_7H_6)[53] and the propargyl radical ($C_3H_3^\bullet$)[54] have been detected at high fractional abundances of $(2.7 \pm 0.3) \times 10^{-10}$ and $(8.7 \pm 0.7) \times 10^{-9}$, respectively. This proof-of-concept study exposes a benchmark of an unconventional, barrierless reaction involving two resonantly stabilized free radicals (RSFRs) leading to the very first gas-phase preparation of azulene along with its naphthalene isomer (Scheme 1). This route signifies a facile, illustrative mechanism to methodically build-up even more complex,

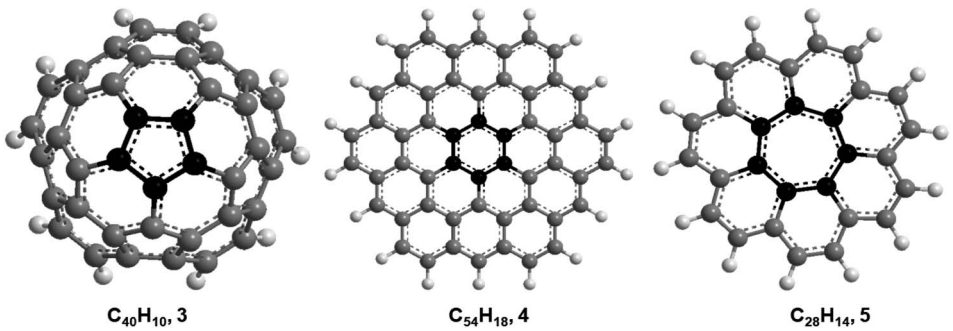

Scheme 2 Representative polycyclic aromatic hydrocarbons (PAHs) carrying five- (left), six (center) and seven-membered rings (right) as in the C_{40} nanobowl ($C_{40}H_{10}$, **3**), circumcoronene ($C_{54}H_{18}$, **4**) and [7]-circulene ($C_{28}H_{14}$, **5**). The incorporation of five-membered rings results in a positive curvature, whereas seven-membered ring inflict a saddle-shaped structures as the result of a positive and negative curvature.

previously elusive functionalized and/or side-chain substituted azulenes in the gas phase through reactions of (alkyl) substituted fulvenallenyl and/or propargyl radicals thus accessing the previously elusive gas phase chemistry of a key class of 10π-Hückel aromatics: azulenes.

Results & discussion

Electron ionization detection

Propargyl ($C_3H_3^{\bullet}$; 39 amu) and fulvenallenyl ($C_7H_5^{\bullet}$; 89 amu) radicals were prepared *in situ* in a resistively heated silicon carbide microreactor *via* pyrolysis of helium-seeded phthalide ($C_8H_6O_2$)[55,56] and propargyl bromide (C_3H_3Br),[40] (Fig. S1 and S3†) respectively. The temperature-dependent ion profiles of the parent ions of the radicals along with the $C_{10}H_8$ isomers are presented in Fig. 1; the neutral reactants and products were ionized by electron ionization at 13 ± 2 eV and sampled by an orthogonal extraction mass spectrometer (Fig. S1†).[57–59] Ion counts at $m/z = 89$ only emerge at temperatures exceeding 1400 ± 50 K. This signal arises predominantly from ionization of the fulvenallenyl radical ($C_7H_5^{\bullet}$) as demonstrated in prior isomer-resolved experiments.[55] Ion signal at both $m/z = 89$ ($C_7H_5^+$) and $m/z = 128$ ($C_{10}H_8^+$) rises as the temperature increases from 1400 to 1700 K, suggesting that the fulvenallenyl radical ($C_7H_5^{\bullet}$; 89 amu) represents a key reactant to form $C_{10}H_8$ (128 amu) isomers. The detection of $C_{10}H_8$ supports earlier modeling work that proposed the reaction of propargyl ($C_3H_3^{\bullet}$) with fulvenallenyl ($C_7H_5^{\bullet}$) as a viable source of naphthalene ($C_{10}H_8$) in combustion environments.[60] However, to support this claim, an isomer-selective analytical technique, *i.e.* soft photoionization, is required to identify the nature of the isomer(s) formed along with their branching ratios.

Photoionization mass spectra

A representative photoionization mass spectrum collected at a photon ionization energy of 9.00 eV is displayed in Fig. 2 for the reaction of the fulvenallenyl ($C_7H_5^{\bullet}$; 89 amu) radical with the propargyl ($C_3H_3^{\bullet}$; 39 amu) radical. These radicals were generated *in situ* in the microreactor at 998 ± 10 K *via* pyrolysis of helium-seeded trichloromethyl-benzene ($C_7H_5Cl_3$) – accounting for the higher yields of fulvenallenyl from trichloromethyl-benzene compared to phthalide pyrolysis[56] – and propargyl bromide (C_3H_3Br),[40] respectively (Fig. S2, S3† and 2c). Control experiments were also carried out by helium-seeding only the trichloromethyl-benzene precursor at 298 K (Fig. 2a). Only ion counts at m/z = 194 ($C_7H_5{}^{35}Cl_3^+$), 195 ($^{13}CC_6H_5{}^{35}Cl_3^+$), 196 ($C_7H_5{}^{35}Cl_2{}^{37}Cl^+$), 197 ($^{13}CC_6H_5{}^{35}Cl_2{}^{37}Cl^+$), 198 ($C_7H_5{}^{35}Cl^{37}Cl_2^+$), 199 ($^{13}CC_6H_5{}^{35}Cl^{37}Cl_2^+$) and 200 ($C_7H_5{}^{37}Cl_3^+$) were detected. When the temperature rises to 998 ± 10 K, the aforementioned ion counts of the trichloromethyl-benzene precursor disappear (Fig. 2b), indicating its quantitative decomposition. The stepwise elimination of chlorine (Cl) atoms from the trichloromethyl-benzene precursor with an increasing temperature of the microreactor is evident from the mass spectra (marked in green in Fig. 2b, c and S4–S7†); as products of the self-recombination of $C_7H_5^{\bullet}$ (89 amu), C_7H_4 (88 amu) and/or C_7H_3 (87 amu), prominent ion peaks emerge at m/z = 174 ($C_{14}H_6^+$), 176 ($C_{14}H_8^+$), and 178 ($C_{14}H_{10}^+$) (Fig. S8†). Once propargyl bromide (C_3H_3Br) is introduced to the reactor, ion counts at $m/z = 39$, 78, 128 and 129 (Fig. 2c and d) emerge; these can be associated with $C_3H_3^{\bullet}$ (39 amu), C_6H_6 (78 amu), $C_{10}H_8$ (128 amu) and $^{13}CC_9H_8$ (129 amu), which are clearly absent in the control experiments (Fig. 2a and b). It shall be highlighted

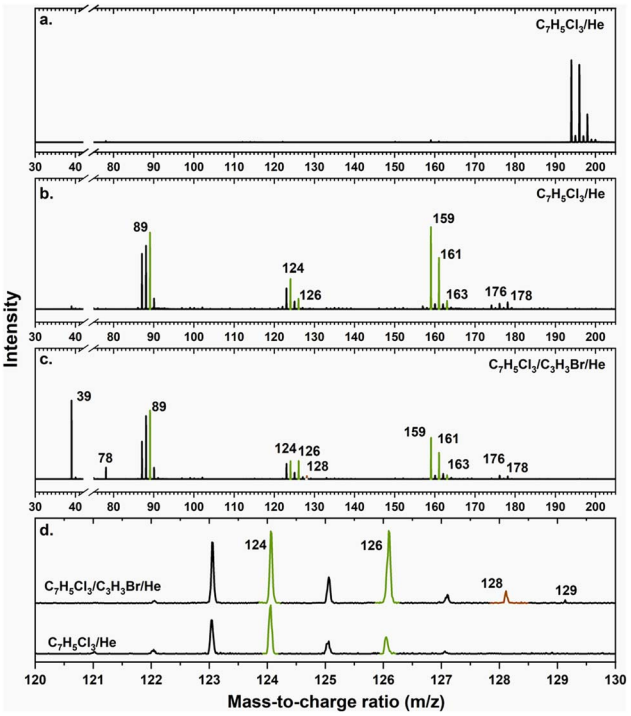

Fig. 2 Mass spectra recorded at the photoionization energy of 9.00 eV. (a) Trichloromethyl-benzene ($C_7H_5Cl_3$)/helium (He) system at 373 ± 10 K; (b) trichloromethyl-benzene ($C_7H_5Cl_3$)/helium (He) system at 998 ± 10 K; (c) trichloromethyl-benzene ($C_7H_5Cl_3$)/propargyl bromide (C_3H_3Br) system at 998 ± 10 K; and (d) magnified comparison of $m/z = 128$ between the reaction and control experiments. The signal at $m/z = 128$ is highlighted in red.

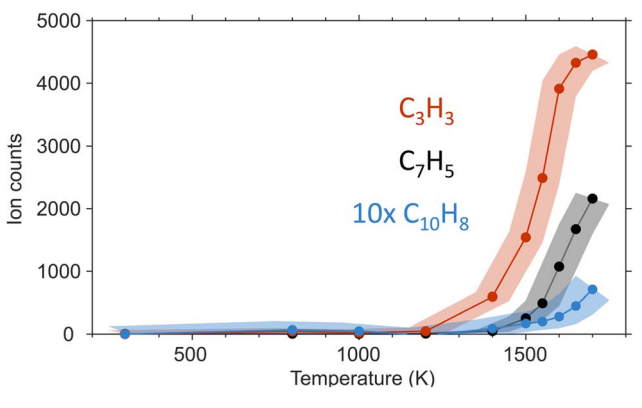

Fig. 1 Temperature-dependent ion count profiles. The red, black and blue lines exhibit respectively ion counts of propargyl ($C_3H_3^{\bullet}$; 39 amu), fulvenallenyl ($C_7H_5^{\bullet}$; 89 amu) radicals and $C_{10}H_8$ isomers (128 amu) in various temperatures in experiments. Error bars include uncertainties in the temperature and shot-to-shot reproducibility.

that a previous investigation of the propargyl radical self-reaction exploiting a chemical micro reactor did not result in any molecular mass growth processed beyond benzene and its acyclic C_6H_6 (78 amu) isomers.[61] Consequently, accounting then for the molecular weight of reactants and the product, signal at $m/z = 128$ ($C_{10}H_8^+$) originates from the reaction of the fulvenallenyl radical ($C_7H_5^\bullet$, $m/z = 89$) with the propargyl radical ($C_3H_3^\bullet$, $m/z = 39$) (Fig. 2d).

Photoionization efficiency (PIE) curves

With the detection of a hydrocarbon molecule of the molecular formula $C_{10}H_8$ (128 amu) formed *via* the fulvenallenyl ($C_7H_5^\bullet$) – propargyl ($C_3H_3^\bullet$) radical–radical reaction, we are focusing now our attention to the elucidation of the structural isomer(s) synthesized in this reaction. This requires a detailed analysis of the photoionization efficiency (PIE) curve, which reports the intensity of the ion at m/z of 128 ($C_{10}H_8^+$) as a function of the photon energy from 7.20 to 9.00 eV.

First, the experimental PIE curve (black) of $m/z = 89$ ($C_7H_5^+$) in trichloromethyl-benzene ($C_7H_5Cl_3$)/propargyl bromide (C_3H_3Br) system is shown in Fig. 3a, along with experimental PIE curve (orange) of fulvenallenyl ($C_7H_5^\bullet$, $m/z = 89$) generated from phthalide pyrolysis (Fig. S9–S10†).[56,62,63] The onset of the ion counts at 8.20 ± 0.05 eV is consistent with the adiabatic ionization energy of fulvenallenyl ($C_7H_5^\bullet$) of 8.19 ± 0.02 eV;[56,63] further, both PIE curves match exceptionally well revealing that fulvenallenyl is generated from both the trichloromethyl-benzene and phthalide precursors (Fig. 3a and S11†). Second, the experimentally collected PIE curve at $m/z = 128$ is displayed in Fig. 3b (black) and overlayed with the reference curves of the $C_{10}H_8$ isomers azulene (blue) and naphthalene (green), as well as the ^{13}C-isotopic signal $^{13}CC_9H_7$ from $m/z = 127$. The experimental PIE curve can be accurately replicated by a linear combination of the PIE curves of azulene ($C_{10}H_8$), naphthalene ($C_{10}H_8$) and the natural ^{13}C contribution of the $C_{10}H_7^\bullet$ radical(s) ($^{13}CC_9H_7$) with the PIE curve of $m/z = 127$ displayed in Fig. S5.† Overall, the onset of ion counts of the experimental PIE curve at 7.40 ± 0.05 eV agrees exceptionally well with the adiabatic ionization energy (IE) of azulene recorded in the present work (IE = 7.41 ± 0.02 eV, Fig. S12b†),[64] while the contribution of naphthalene (IE = 8.14 ± 0.01 eV)[64,65] becomes evident at photon energies of 8.15 ± 0.05 eV and higher. Therefore, our experimental data provide compelling evidence on the formation of both azulene and naphthalene under our experimental conditions. Accounting for the absolute photoionization cross sections,[65] branching ratios of azulene *versus* naphthalene are derived to be 5.7 ± 0.7% *versus* 94.3 ± 11.3%. We would like to stress that the inclusion of monocyclic $C_{10}H_8$ isomers carrying, *e.g.*, a benzene ring with a C_4H_3 side chain such as 4-phenylvinylacetylene (IE = 8.25 ± 0.05 eV) and *trans*-1-phenylvinylacetylene (IE = 8.20 ± 0.05 eV),[66] cannot replicate the experimentally derived PIE at $m/z = 128$; only upper limits of 4-phenylvinylacetylene and *trans*-1-phenylvinylacetylene of up to 2% of the ion counts can result in acceptable fits (Fig. S13†). These conclusions are also supported by the analysis of the PIE curve at $m/z = 129$ which results from ^{13}C isotopes (10 × 1.109% natural abundance) of $C_{10}H_8$ isomers, azulene and naphthalene (Fig. 3c and S14†).

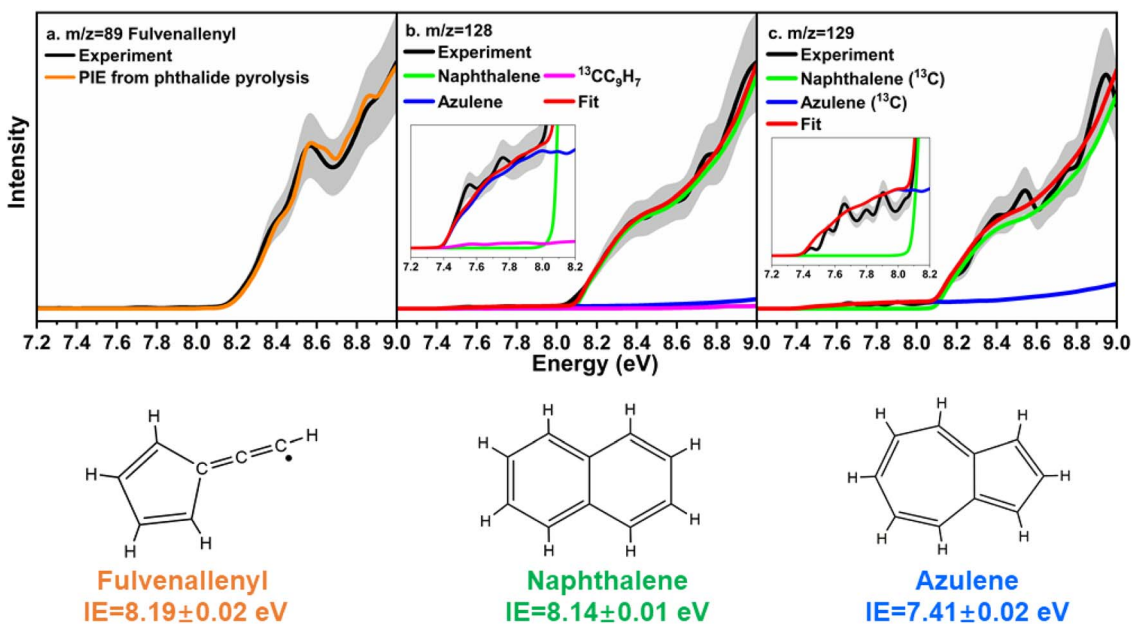

Fig. 3 Experimental and reference photoionization efficiency (PIE) curves for species at $m/z = 89$ (a), 128 (b) and 129 (c) in the trichloromethyl-benzene ($C_7H_5Cl_3$)/propargyl bromide (C_3H_3Br) system at 998 ± 10 K. The overall error bars consist of three parts: ±10% based on the accuracy of the photodiode, ±5% considering the injection stability and a 1σ error of the PIE curve averaged over the individual scans. The color-coded lines refer to the reference PIE curves of azulene (blue) and naphthalene (green) isomers. The orange line means experimental PIE curve of fulvenallenyl generated from the traditional phthalide pyrolysis revealing an excellent match with fulvenallenyl prepared from trichloromethyl-benzene. The red lines show the overall fit *via* the linear combination of the reference curves.

Potential energy surfaces

With the explicit experimental detection of azulene and naphthalene isomers ($C_{10}H_8$) formed *via* the gas phase reaction of the fulvenallenyl radical ($C_7H_5^{\bullet}$) with the propargyl radical ($C_3H_3^{\bullet}$) in the gas phase, it is our objective to unravel the underlying reaction mechanisms. In case of complex systems, it is of advantage to combine the experimental results with electronic structure calculations (Section 6†) to explore synthetic routes to naphthalene (**p1**) and azulene (**p2**) with relative energies of the products, intermediates and transition states calculated with an accuracy of ± 4 kJ mol^{-1}. Fig. 4 illustrates resonance structures of the fulvenallenyl and propargyl radicals depicting their singly occupied molecular orbitals (SOMO) and distribution of the electron spin density. Fulvenallenyl can be considered as an analog of propargyl with the five-membered ring moiety of fulvenallenyl substituted by the CH_2 group of propargyl. While the propargyl radical ($C_3H_3^{\bullet}$) possesses only *two* resonance structures with the unpaired electron delocalized between the CH (tail) and CH_2 (head) ends, fulvenallenyl ($C_7H_5^{\bullet}$) features *six* resonance structures, four of which are symmetrically unique with the radical distributed between the exocyclic CH end and each of the five carbon atoms in the five-membered ring. This is supported by the structure of the singly occupied molecular orbital (SOMO) and the computed spin distribution which shows the highest spin density in the *ipso* position in the ring followed by the terminal, exocyclic methylidyne moiety (CH) carbon and the carbon atoms in the *meta* positions in the ring. The *ortho* carbon atoms in the ring carry the lowest – by the absolute value – spin density. Therefore, there are four chemically distinct sites for the propargyl radical addition to fulvenallenyl, although the addition to the *ortho* positions is anticipated to be least likely. Altogether, considering the head–tail delocalization of spin density in propargyl, the fulvenallenyl – propargyl reaction can be initiated *via* eight distinct entrance channels.

Naphthalene formation

The calculations of the relevant $C_{10}H_8$ potential energy surface (PES) portray that these eight entrance channels can be subdivided into two groups, where the rearrangements of the initial complexes formed in each of the group appear to have relatively low barriers and thus are faster than the competing isomerization reactions (Fig. 5a and b). The first group (Fig. 5a) includes propargyl ($C_3H_3^{\bullet}$) tail addition to the *ipso*, *ortho* and *meta* positions in the five-membered ring of fulvenallenyl ($C_7H_5^{\bullet}$) together with propargyl ($C_3H_3^{\bullet}$) head addition to the CH end (tail) of fulvenallenyl ($C_7H_5^{\bullet}$); these additions lead to intermediates **i1**, **i2**, **i13** and **i14**, respectively. Here, the ring additions are interconnected by facile migrations of the propargyl moiety between neighboring carbon atoms in the ring, whereas the initial complex of the head addition easily interconverts to the complex formed by the tail addition to the *ipso* position by the $C_3H_3^{\bullet}$ rebound occurring *via* a six-membered ring transition state (TS). Seemingly, the second group (Fig. 5b) combines propargyl head additions to the carbon atoms in the *ipso*, *ortho* and *meta* positions with the tail addition to the tail of fulvenallenyl ($C_7H_5^{\bullet}$) accessing intermediates **i15**, **i16**, **i17** and **i18**, respectively; from these, the propargyl can easily rebound from the initial complex for the *ipso*-ring addition to the initial complex for the tail-to-tail addition. Fig. 5 compiles only the most favorable pathways leading to naphthalene (**p1**), azulene (**p2**), fulvalene (**p3**) and 5-methylene-5*H*-indene (**p4**). The preferential pathways to naphthalene (Fig. 5a, pink) initiate from the initial complexes for tail addition to the *ipso* and *ortho* carbons in the ring, *i.e.*, intermediates **i1** and **i2**, residing 216 and 245 kJ mol^{-1} lower in energy than the reactants, respectively. Although **i2** is thermodynamically more

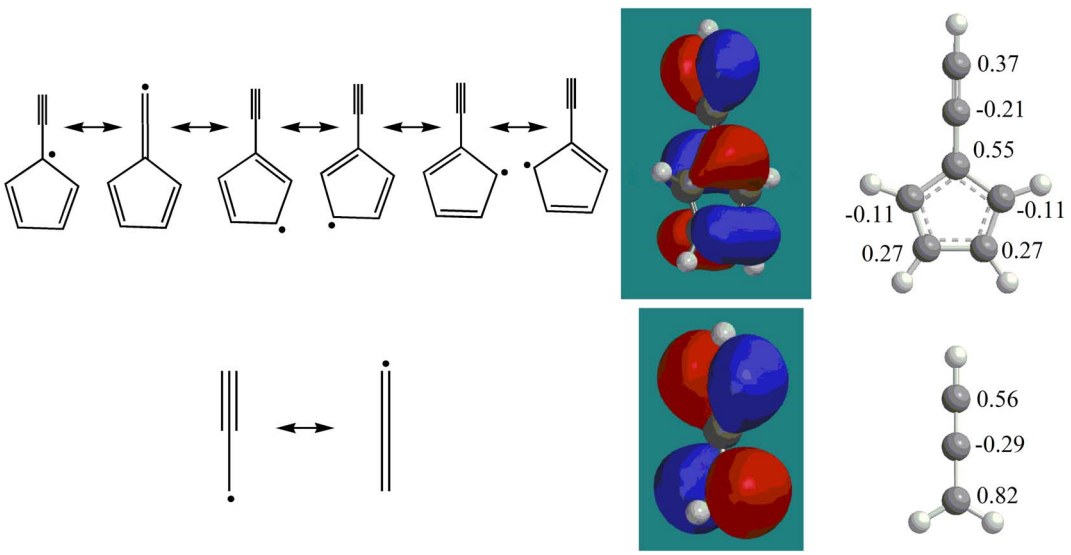

Fig. 4 Schematic of electron distribution including computed partial charges on individual carbon atoms, singly occupied molecular orbitals (SOMO) and spin density distribution including computed spin densities on C atoms in fulvenallenyl ($C_7H_5^{\bullet}$, top row) and propargyl ($C_3H_3^{\bullet}$, bottom row) radicals.

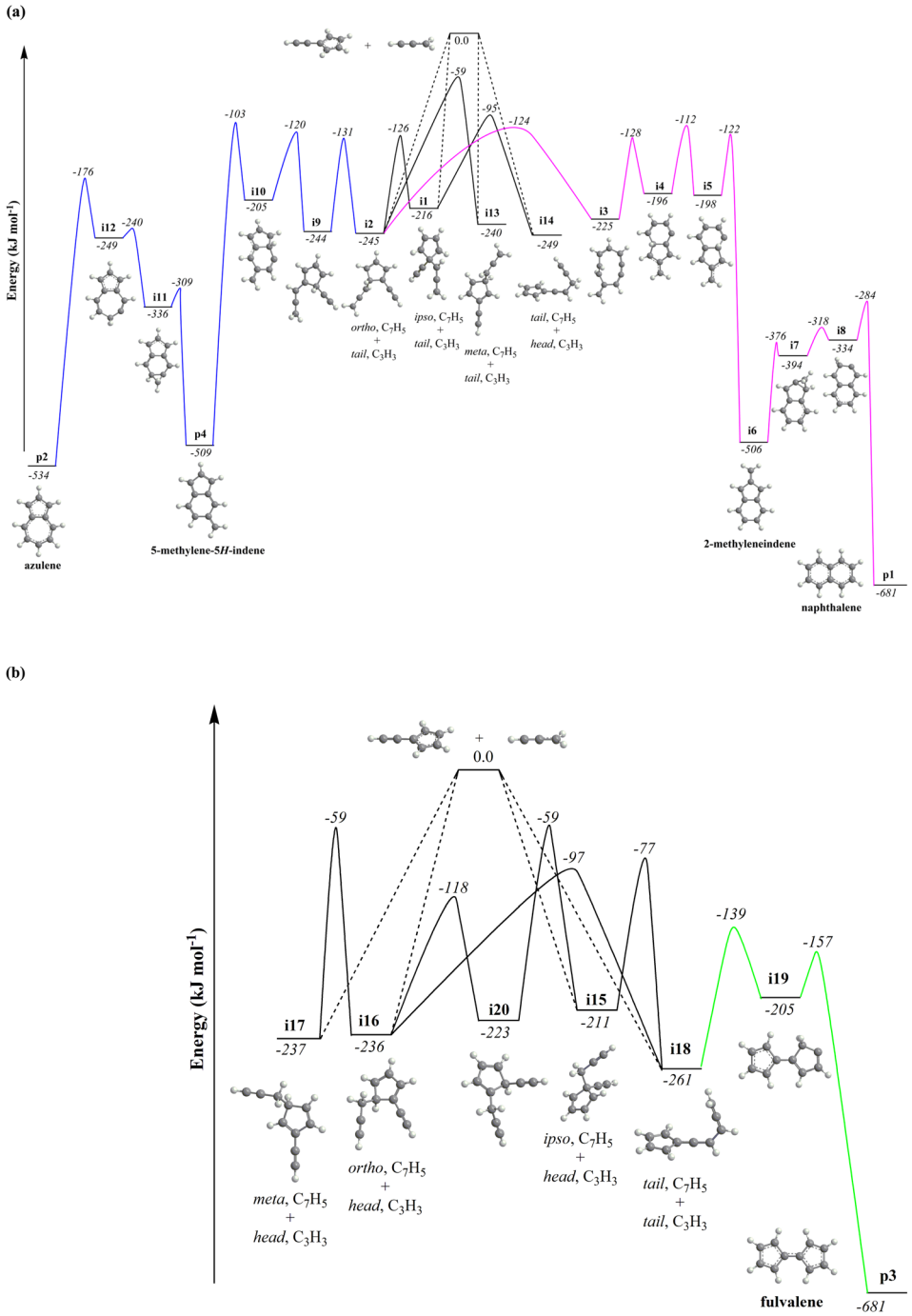

Fig. 5 Most favorable reaction pathways of the reaction of fulvenallenyl ($C_7H_5^\bullet$) with propargyl ($C_3H_3^\bullet$) (a) to naphthalene and azulene and (b) to fulvalene. See Fig. S15 in ESI† for structures of representative transition states.

stable than **i1**, it is likely that the formation of **i2** is kinetically hindered because of the low spin density on the *ortho* carbon atom. Nevertheless, **i1** rearranges to **i2** *via* a relatively low barrier of 90 kJ mol^{-1}. The pathway from **i2** to naphthalene involves cyclization to a ten-membered ring with the initial five-membered ring being open (**i2** → **i3**), contraction of the ten-membered ring to a bicyclic structure featuring fused six- and five-membered rings with an out-of-ring methylene (CH_2) group (**i3** → **i4**), two consecutive 1,2-hydrogen shifts around the six-membered ring (**i4** → **i5** → **i6**), leading to 2-methyleneindene (**i6**), insertion of the CH_2 group in the five-membered ring leading to its expansion to a six-membered ring (**i6** → **i7** → **i8**) and finally, 1,2-hydrogen migration **i8** → **p1** to naphthalene. The highest energy transition state along the pathway from **i2** to naphthalene resides 112 kJ mol^{-1} lower in energy than the separated reactants and corresponds to the hydrogen migration step **i4** → **i5**.

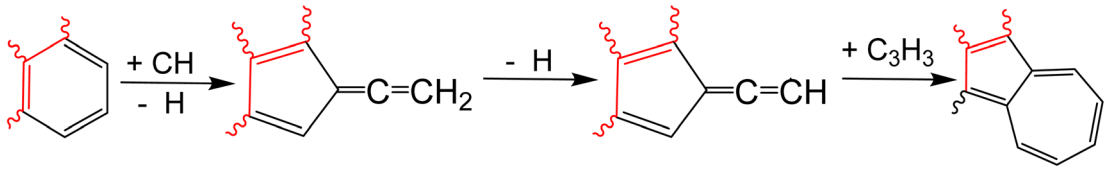

Fig. 6 Schematic representation of versatile molecular mass growth processes to PAH-embedded azulene units involving the novel Fulvenallenyl Addition Cyclization Aromatization (FACA) reaction mechanism. The waved lines symbolize the chemical bonding to extended aromatic systems.

Azulene formation

Alternatively, **i2** can give rise to azulene (Fig. 5a, blue) *via* a multistep pathway featuring 1,2-hydrogen migration (**i2** → **i9**), a six-membered ring closure (**i9** → **i10**), another hydrogen shift (**i10** → **p4**) resulting in a rather stable 5-methylene-5*H*-indene species **p4**. 5-Methylene-5*H*-indene can further be subjected to insertion of the out-of-ring methylene group to the six-membered ring expanding it to a seven-membered ring (**p4** → **i11** → **i12**), with a hydrogen shift completing the formation of azulene (**i12** → **p2**), which is 534 kJ mol^{-1} exoergic with respect to the reactants. The highest in energy transition state along this pathway corresponds to the hydrogen shift **i10** → **p4**. Interestingly, in both routes from **i2** to naphthalene and azulene, the critical ring closure steps leave an out-of-ring methylene group, which later inserts either into five- or six-membered ring. This mechanism is reminiscent of the so-called methylene walk mechanism in a hydrogen atom assisted isomerization of azulene to naphthalene occurring on the $C_{10}H_9^{\bullet}$ PES.[67,68] The computationally predicted difference in enthalpies of formation of naphthalene and azulene of 147 ± 4 kJ mol^{-1} agrees closely with the NIST derived value of 158 ± 10 kJ mol^{-1}.

Fulvalene formation

The channels proceeding through the second group of entrance channels represented by the tail-to-tail addition forming **i18** provide a facile route to fulvalene (IE = 8.70 eV,[69] Fig. 5b, green). In particular, the side chain in **i18** undergoes a five-membered ring closure to **i19**, where a 1,2-shift from the CH_2 moiety to the bare carbon atom in the newly formed ring produce fulvalene (**p3**). Here, the highest energy along the **i18** → **i19** → **p3** pathway corresponds to the ring closure step and is located 139 kJ mol^{-1} below the initial reactants.

Statistical calculations

It should be also noted that isomerization channels connecting the first and second groups of the initial complexes represented, *e.g.*, by the tail addition of propargyl to the ring (**i1**, *ipso*) and to the tail of fulvenallenyl (**i18**) are only weakly interconnected. Although pathways between the two groups exist, they are not kinetically competitive. We carried out product branching ratio calculations for these two distinct entrance channel groups at various temperatures and pressures. Fig. S16† illustrates the results for the pressure of 0.01 atm representative for the reactive zone of the microreactor. One can see that for the propargyl tail addition to the ring or its head addition to the tail of fulvenallenyl at high temperatures relevant to the conditions in the microreactor, naphthalene (**p1**) is the prevailing product followed by 5-methylene-5*H*-indene (**p4**), fulvalene (**p3**) and azulene (**p2**). Alternatively, the second group of entrance channels (tail-to-tail and propargyl head to fulvenallenyl ring) is expected to predominantly form fulvalene. The experimental branching ratio of 5.7 ± 0.7% (azulene) *versus* 94.3 ± 11.3% (naphthalene) at 998 ± 10 K favors the gas-phase formation of the naphthalene isomer. Considering only the primary reaction products, the calculated branching ratio of azulene to naphthalene at 1000 K for the case of head-to-tail and tail-to-ring group of additions is 1.8% *vs.* 98.2%, whereas the tail-to-tail and head-to-ring additions should produce negligibly small amounts of both naphthalene and azulene. In the meantime, neither fulvalene nor 5-methylene-5*H*-indene (IE = 7.34 eV, Section 6†) could be detected experimentally. It is likely that these products are rapidly converted to naphthalene and/or azulene *via* a hydrogen assisted isomerization.[70–72] Besides, it was reported that fulvalene is preferred in the high-temperature condition over 1000 K.[67,73] In particular, considering the reaction kinetics on the $C_{10}H_9^{\bullet}$ PES explored in the previous theoretical studies,[67] once can anticipated that the hydrogen atom plus fulvalene reaction would predominantly produce naphthalene plus atomic hydrogen *via* the spiran mechanism, whereas atomic hydrogen plus 5-methylene-5*H*-indene would preferentially form azulene and a hydrogen atom by methylene insertion into the six-membered ring. Within this framework, the overall azulene to naphthalene branching ratio can be determined taking account both the primary reaction and secondary hydrogen atom assisted isomerization and considering the branching between the two groups of entrance channels as a variable parameter. Taking this entrance channel group branching as 50/50, we obtain the azulene/naphthalene yields as 10.9/89.1; the experimental branching ratio can be reproduced with the entrance channel branching of 31/69. Accurate calculations of the branching of various entrance channels and absolute temperature- and pressure-depending rate constants for the formation of various products is a demanding task which can be achieved using variable reaction coordinate transition state theory (VRC-TST) and thus is left for a future study.

Conclusion & outlook

The experimental and computational exploration of the reaction of two resonantly stabilized free radicals – fulvenallenyl

($C_7H_5^\bullet$) and propargyl ($C_3H_3^\bullet$) – provided persuasive evidence of the very first gas-phase synthesis of the 10π aromatic azulene molecule ($C_{10}H_8$) *via* the novel Fulvenallenyl Addition Cyclization Aromatization (FACA) reaction mechanism. Eight distinct entrance channels have been identified including head (CH_2) additions of propargyl to the tail (terminal CH) of fulvenallenyl and tail (CH) additions of propargyl to the ring of fulvenallenyl as well as tail-to-tail and head-to-ring additions. The additions from the first group preferentially form naphthalene along with 5-methylene-5*H*-indene, fulvalene and azulene, whereas the second group of additions predominantly forms fulvalene under high temperature conditions. Under the experimental conditions, 5-methylene-5*H*-indene and fulvalene can be rapidly converted to azulene and naphthalene, respectively, *via* hydrogen-assisted isomerization. Within this framework, the experimental azulene-to-naphthalene branching ratio can be reproduced assuming a nearly 2 : 1 branching between the entrance channel tail-to-tail plus head-to-ring and head-to-tail plus tail-to-ring groups. Note that a previous study of the fulvenallenyl – propargyl system exploiting infrared (IR)/ultraviolet (UV) ion dip spectroscopy only detected the naphthalene isomer, but not azulene.[56] The unsuccessful identification of azulene by Horsch *et al.*[74] is likely the direct consequence of the IR/UV detection method, which makes an identification of products at a level of less than about 10% very challenging.[75]

The reaction mechanism elucidated here provides a versatile concept introducing an azulene moiety, *i.e.*, a seven-membered ring adjacent to a five membered ring, into polycyclic aromatic systems *via* molecular mass growth processes involving the reaction of a fulvenallenyl moiety with propargyl radicals (Fig. 6). Commencing with the bimolecular reaction of a PAH-embedded benzene ring with a methylidyne radical (CH), a six-membered ring can be effectively converted into a fulvenallene moiety as long as the embedded benzene ring has three adjacent hydrogen atoms demonstrated in the crossed molecular beam reaction of benzene (C_6H_6) with methylidyne (CH).[51] Hydrogen atom loss from the exocyclic CCH_2 functional group through photodissociation or abstraction leads to the PAH-embedded fulvenallenyl unit, which can then react with a propargyl radical to the azulene moiety embedded in an aromatic system. It is important to highlight that the last step requires a third body collisional stabilization – as provided in our microreactor by the helium buffer gas – to transfer the internal energy to the third body collider or a potential radiative stabilization under interstellar conditions. Therefore, hydrocarbon-rich atmospheres of planets and their moons such as Titan present ideal natural laboratories to allow barrierless and exoergic reactions to, *e.g.*, azulene, which are terminated by stabilization through collision with a bath molecule such as molecular nitrogen in case of Titan. Even in combustion systems, extensive molecular mass growth processes could lead to PAHs carrying seven-membered rings as a critical prerequisite of exotic 'saddle-shaped' aromatic systems with both a positive and negative curvature of the carbon backbone. Overall, the isomer selective identification of aromatic molecules formed *via* the reaction of (resonantly stabilized) hydrocarbon radicals exploiting tunable synchrotron light has just scratched the surface and is expected to enhance our fundamental knowledge on molecular mass growth processes to aromatic structures on the fundamental, microscopic level in our Universe.

Data availability

Essential data are provided in the main text and the ESI.† Additional data can be available from the corresponding author upon reasonable request.

Author contributions

L. Z. and N. H. designed the experiments; W. L. carried out the experimental measurements in NSRL and performed the data analysis; D. C. and M. S. M. carried out the experimental measurements at Sandia and performed the data analysis. L. Z., J. Y. and N. H. supervised the experiments; A. N. M. and A. M. M. carried out the theoretical analysis; all authors discussed the data. L. Z., R. I. K., N. H., and A. M. M. wrote the manuscript.

Conflicts of interest

The authors declare no competing interest.

Acknowledgements

The authors are grateful for the funding supports from National Natural Science Foundation of China (22173091). RIK acknowledges support from the U.S. Department of Energy, Basic Energy Sciences DE-FG02-03ER15411. ANM and AMM acknowledge support from the U.S. Department of Energy, Basic Energy Sciences DE-FG02-04ER15570. This works is based on user proposal 2022-HLS-PT-004982 (RIK, LZ). DC, MSM, NH acknowledge support from the U.S. Department of Energy, Office of Science, Office of Basic Energy Sciences, Division of Chemical Sciences, Geosciences and Biosciences. MSM was supported by the Department of Energy, Office of Science, Office of Workforce Development for Teachers and Scientists (WDTS) under the Science Undergraduate Laboratory Internships Program (SULI). Sandia National Laboratories is a multimission laboratory managed and operated by the National Technology and Engineering Solutions of Sandia, LLC, a wholly owned subsidiary of Honeywell International, Inc., for the U.S. DOE's National Nuclear Security Administration under contract DENA0003525. This paper describes objective technical results and analysis. Any subjective views or opinions that might be expressed in the paper do not necessarily represent the views of the U.S. DOE or the U.S. Government.

References

1 A. St. Pfau and P. A. Plattner, Pfau-Plattner azulene synthesis, *Helv. Chim. Acta*, 1939, **22**, 202.
2 N. Ogawa, Y. Yamaoka, H. Takikawa, K. I. Yamada and K. Takasu, Helical nanographenes embedded with

contiguous azulene units, *J. Am. Chem. Soc.*, 2020, **142**, 13322–13327.
3 A. Costa and A. López-Castillo, Prediction of azulene-based nanographene-like materials, *Diamond Relat. Mater.*, 2021, **112**, 108235.
4 C. G. V. de la Garza, G. L. García, E. M. Olmedo, E. R. Peña and S. Fomine, Electronic structure of isomeric graphene nanoflakes, *Comput. Theor. Chem.*, 2018, **1140**, 125–133.
5 I. A. Popov and A. I. Boldyrev, Chemical bonding in coronene, isocoronene, and circumcoronene, *Eur. J. Org Chem.*, 2012, **18**, 3485–3491.
6 X. Zheng, L. Liu, C. Yang, Y. He, J. Chen and W. Tian, Modulation of the second order nonlinear optical properties of helical graphene nanoribbons through introducing azulene defects or/and BN units, *Chem. Res. Chin. Univ.*, 2021, **38**, 974–984.
7 Y. He, J. Chen, X. Zheng, X. Xu, W. Li, L. Yang and W. Tian, Spiral graphene nanoribbons with azulene defects as potential nonlinear optical materials, *ACS Appl. Nano Mater.*, 2019, **2**, 1648–1654.
8 H. Gao, C. Ge, B. Hou, H. Xin and X. Gao, Incorporation of 1,3-free-2,6-connected azulene units into the backbone of conjugated polymers: improving proton responsiveness and electrical conductivity, *ACS Macro Lett.*, 2019, **8**, 1360–1364.
9 A. F. Rahman, S. Bhattacharya, X. Peng, T. Kimura and N. Komatsu, Unexpectedly large binding constants of azulenes with fullerenes, *Chem. Commun.*, 2008, **10**, 1196–1198.
10 J. W. Martin, C. de Tomas, I. Suarez-Martinez, M. Kraft and N. A. Marks, Topology of disordered 3D graphene networks, *Phys. Rev. Lett.*, 2019, **123**, 116105.
11 G. N. Sastry, E. D. Jemmis, G. Mehta and S. R. Shah, Synthetic strategies towards C_{60}. Molecular mechanics and MNDO study on sumanene and related structures, *J. Chem. Soc., Perkin Trans. 2*, 1993, **10**, 1867–1871.
12 C. W. Bauschlicher, The infrared spectra of nonplanar polycyclic aromatic hydrocarbons with five- or seven-membered rings, *Chem. Phys.*, 2015, **448**, 43–52.
13 H. Xin, B. Hou and X. Gao, Azulene-based π-functional materials: design, synthesis, and applications, *Acc. Chem. Res.*, 2021, **54**, 1737–1753.
14 L. Ou, Y. Zhou, B. Wu and L. Zhu, The unusual physicochemical properties of azulene and azulene-based compounds, *Chin. Chem. Lett.*, 2019, **30**, 1903–1907.
15 X. Yang, F. Rominger and M. Mastalerz, Contorted polycyclic aromatic hydrocarbons with two embedded azulene units, *Angew. Chem., Int. Ed.*, 2019, **58**, 17577–17582.
16 A. Artigas, D. Hagebaum-Reignier, Y. Carissan and Y. Coquerel, Visualizing electron delocalization in contorted polycyclic aromatic hydrocarbons, *Chem. Sci.*, 2021, **12**, 13092–13100.
17 F. Wang, Y. Lai and M. Han, Stimuli-responsive conjugated copolymers having electro-active azulene and bithiophene units in the polymer skeleton: effect of protonation and p-doping on conducting properties, *Macromolecules*, 2004, **37**, 3222–3230.
18 L. Cristian, I. Sasaki, P. G. Lacroix and B. Donnadieu, Donating strength of azulene in various azulen-1-yl-substituted cationic dyes: application in nonlinear optics, *Chem. Mater.*, 2004, **16**, 3543–3551.
19 G. P. van der Zwet and L. J. Allamandola, Polycyclic aromatic hydrocarbons and the diffuse interstellar bands, *Astron. Astrophys.*, 1985, **146**, 76–80.
20 A. A. Ruth, E. K. Kim and A. Hese, The S_0-S_1 cavity ring-down absorption spectrum of jet-cooled azulene: dependence of internal conversion on the excess energy, *Phys. Chem. Chem. Phys.*, 1999, **1**, 5121–5128.
21 A. Menon, G. Leon, J. Akroyd and M. Kraft, A density functional theory study on the kinetics of seven-member ring formation in polyaromatic hydrocarbons, *Combust. Flame*, 2020, **217**, 152–174.
22 F. Cataldo, D. A. García-Hernández and A. Manchado, Petroleum, coal and other organics in space, *Astrophys. Space Sci.*, 2020, **365**, 5–18.
23 I. Cherchneff, The formation of polycyclic aromatic hydrocarbons in evolved circumstellar environments, *EAS Publ. Ser.*, 2011, **46**, 177–189.
24 L. Zhao, S. Doddipatla, R. I. Kaiser, W. Lu, O. Kostko, M. Ahmed, L. B. Tuli, A. N. Morozov, A. H. Howlader, S. F. Wnuk, A. M. Mebel, V. N. Azyazov, R. K. Mohamed and F. R. Fischer, Gas-phase synthesis of corannulene – a molecular building block of fullerenes, *Phys. Chem. Chem. Phys.*, 2021, **23**, 5740–5749.
25 C. Jäger, F. Huisken, H. Mutschke, I. L. Jansa and T. Henning, Formation of polycyclic aromatic hydrocarbons and carbonaceous solids in gas-phase condensation experiments, *Astrophys. J.*, 2009, **696**, 706–712.
26 C. S. Contreras and F. Salama, Laboratory investigations of polycyclic aromatic hydrocarbon formation and destruction in the circumstellar outflows of carbon stars, *Astrophys. J., Suppl. Ser.*, 2013, **208**, 6–23.
27 S. Fascella, C. Cavallotti, R. Rota and S. Carra, From PAHs to solid carbon, *EAS Publ. Ser.*, 2011, **46**, 293–304.
28 R. I. Kaiser and N. Hansen, An aromatic universe-A physical chemistry perspective, *J. Phys. Chem. A*, 2021, **125**, 3826–3840.
29 A. Ricca, J. C. W. Bauschlicher and L. J. Allamandola, The infrared spectroscopy of polycyclic aromatic hydrocarbons with five- and seven-membered fused ring defects, *Astrophys. J.*, 2011, **729**, 94–102.
30 T. Nozoe, S. Seto, S. Matsumura and T. Asano, Synthesis of azulene derivatives from troponoids and cyanoacetic ester, *Proc. Jpn. Acad.*, 1956, **32**, 339–343.
31 T. Nozoe, K. Takase, K. Kato and T. Nogi, The reaction of 2-arylsulfonyloxytropones and active methylene compounds: the formation of 8-hydroxy-2H-cyclohepta[b]furan-2-one and 2-amino-8H-cyclohepta[b]furan-8-one derivatives, *Tetrahedron*, 1971, **27**, 6023–6035.
32 J. Ma, Y. Fu, E. Dmitrieva, F. Liu, H. Komber, F. Hennersdorf, A. A. Popov, J. J. Weigand, J. Liu and X. Feng, Helical nanographenes containing an azulene unit: synthesis, crystal structures, and properties, *Angew. Chem., Int. Ed.*, 2020, **59**, 5637–5642.

33 A. Ong, T. Tao, Q. Jiang, Y. Han, Y. Ou, K. Huang and C. Chi, Azulene-fused acenes, *Angew. Chem., Int. Ed.*, 2022, **134**, e202209286.

34 C. Duan, J. Zhang, J. Xiang, X. Yang and X. Gao, Azulene-embedded [n]helicenes (n=5, 6 and 7), *Angew. Chem., Int. Ed.*, 2022, **61**, e202201494.

35 K. Kawai, K. Kato, L. Peng, Y. Segawa, L. T. Scott and K. Itami, Synthesis and structure of a propeller-shaped polycyclic aromatic hydrocarbon containing seven-membered rings, *Org. Lett.*, 2018, **20**, 1932–1935.

36 M. Schnitzlein, C. Mützel, K. Shoyama, J. M. Farrell and F. Würthner, PAHs containing both heptagon and pentagon: corannulene extension by [5 + 2] annulation, *Eur. J. Org Chem.*, 2022, **5**, e202101273.

37 Z. Qiu, S. Asako, Y. Hu, C. W. Ju, T. Liu, L. Rondin, D. Schollmeyer, J. S. Lauret, K. Mullen and A. Narita, Negatively curved nanographene with heptagonal and [5] helicene units, *J. Am. Chem. Soc.*, 2020, **142**, 14814–14819.

38 J. I. Urgel, M. Di Giovannantonio, Y. Segawa, P. Ruffieux, L. T. Scott, C. A. Pignedoli, K. Itami and R. Fasel, Negatively curved warped nanographene self-assembled on metal surfaces, *J. Am. Chem. Soc.*, 2019, **141**, 13158–13164.

39 Q. Fan, D. Martin-Jimenez, D. Ebeling, C. K. Krug, L. Brechmann, C. Kohlmeyer, G. Hilt, W. Hieringer, A. Schirmeisen and J. M. Gottfried, Nanoribbons with nonalternant topology from fusion of polyazulene: carbon allotropes beyond graphene, *J. Am. Chem. Soc.*, 2019, **141**, 17713–17720.

40 L. Zhao, W. Lu, M. Ahmed, M. V. Zagidullin, V. N. Azyazov, A. N. Morozov, A. M. Mebel and R. I. Kaiser, Gas-phase synthesis of benzene via the propargyl radical self-reaction, *Sci. Adv.*, 2021, **7**, eabf0360.

41 W. Li, L. Zhao and R. I. Kaiser, A unified reaction network on the formation of five-membered ringed polycyclic aromatic hydrocarbons (PAHs) and their role in ring expansion processes through radical-radical reactions, *Phys. Chem. Chem. Phys.*, 2023, **25**, 4141–4150.

42 L. Zhao, R. I. Kaiser, B. Xu, U. Ablikim, M. Ahmed, M. M. Evseev, E. K. Bashkirov, V. N. Azyazov and A. M. Mebel, A unified mechanism on the formation of acenes, helicenes, and phenacenes in the gas phase, *Angew Chem. Int. Ed. Engl.*, 2020, **59**, 4051–4058.

43 J. E. Pollard and R. B. Cohen, Electron-impact ionization time-of-flight mass spectrometer for molecular beams, *Rev. Sci. Instrum.*, 1987, **58**, 32–37.

44 K. Kohse-Höinghaus, P. Oßwald, U. Struckmeier, T. Kasper, N. Hansen, C. A. Taatjes, J. Wang, T. A. Cool, S. Gon and P. R. Westmoreland, The influence of ethanol addition on premixed fuel-rich propene–oxygen–argon flames, *Proc. Combust. Inst.*, 2007, **31**, 1119–1127.

45 L. Ruwe, L. Cai, J. Wullenkord, S. C. Schmitt, D. Felsmann, M. Baroncelli, B. Chen, K. Moshammer, N. Hansen, H. Pitsch and K. Kohse-Höinghaus, Low- and high-temperature study of n-heptane combustion chemistry, *Proc. Combust. Inst.*, 2021, **38**, 405–413.

46 Z. Zhou, X. Du, J. Yang, Y. Wang, C. Li, S. Wei, L. Du, Y. Li, F. Qi and Q. Wang, The vacuum ultraviolet beamline/endstations at NSRL dedicated to combustion research, *J. Synchrotron Radiat.*, 2016, **23**, 1035–1045.

47 A. Goel, P. Hebgen, J. B. V. Sande and J. B. Howard, Combustion synthesis of fullerenes and fullerenic nanostructures, *Carbon*, 2002, **40**, 177–182.

48 D. K. Bohme, PAH and fullerene ions and ion/molecule reactions in interstellar and circumstellar chemistry, *Chem. Rev.*, 1992, **92**, 1487–1508.

49 R. I. Kaiser, D. S. Parker and A. M. Mebel, Reaction dynamics in astrochemistry: low-temperature pathways to polycyclic aromatic hydrocarbons in the interstellar medium, *Annu. Rev. Phys. Chem.*, 2015, **66**, 43–67.

50 M. K. Spencer, M. R. Hammond and R. N. Zare, Laser mass spectrometric detection of extraterrestrial aromatic molecules: mini-review and examination of pulsed heating effects, *Proc. Natl. Acad. Sci. U.S.A.*, 2008, **105**, 18096–18101.

51 C. He, A. M. Thomas, G. R. Galimova, A. N. Morozov, A. M. Mebel and R. I. Kaiser, Gas-phase formation of fulvenallene (C_7H_6) via the Jahn–Teller distorted tropyl (C_7H_7) radical intermediate under single-collision conditions, *J. Am. Chem. Soc.*, 2020, **142**, 3205–3213.

52 G. da Silva, Reaction of benzene with atomic carbon: pathways to fulvenallene and the fulvenallenyl radical in extraterrestrial atmospheres and the interstellar medium, *J. Phys. Chem. A*, 2014, **118**, 3967–3972.

53 J. Cernicharo, R. Fuentetaja, M. Agúndez, R. I. Kaiser, C. Cabezas, N. Marcelino, B. Tercero, J. R. Pardo and P. de Vicente, Discovery of fulvenallene in TMC-1 with the QUIJOTE line survey, *Astron. Astrophys.*, 2022, **663**, L9.

54 M. Agundez, C. Cabezas, B. Tercero, N. Marcelino, J. D. Gallego, P. de Vicente and J. Cernicharo, Discovery of the propargyl radical (CH_2CCH) in TMC-1: one of the most abundant radicals ever found and a key species for cyclization to benzene in cold dark clouds, *Astron. Astrophys.*, 2021, **647**, L10.

55 J. Bouwman, H. R. Hrodmarsson, G. B. Ellison, A. Bodi and P. Hemberger, Five birds with one stone: photoelectron photoion coincidence unveils rich phthalide pyrolysis chemistry, *J. Phys. Chem. A*, 2021, **125**, 1738–1746.

56 F. Hirsch, I. Fischer, S. Bakels and A. M. Rijs, Gas-phase infrared pectra of the C_7H_5 radical and its bimolecular reaction products, *J. Phys. Chem. A*, 2022, **126**, 2532–2540.

57 D. E. Couch, A. J. Zhang, C. A. Taatjes and N. Hansen, Experimental observation of hydrocarbon growth by resonance-stabilized radical–radical chain reaction, *Angew. Chem., Int. Ed.*, 2021, **60**, 27230–27235.

58 K. Moshammer, L. Seidel, Y. Wang, H. Selim, S. M. Sarathy, F. Mauss and N. Hansen, Aromatic ring formation in opposed-flow diffusive 1,3-butadiene flames, *Proc. Combust. Inst.*, 2017, **36**, 947–955.

59 L. Ruwe, K. Moshammer, N. Hansen and K. Kohse-Hoinghaus, Influences of the molecular fuel structure on combustion reactions towards soot precursors in selected alkane and alkene flames, *Phys. Chem. Chem. Phys.*, 2018, **20**, 10780–10795.

60 N. Hansen, B. Yang, M. Braun-Unkhoff, A. Ramirez and G. Kukkadapu, Molecular-growth pathways in premixed

flames of benzene and toluene doped with propyne, *Combust. Flame*, 2022, **243**, 112075.

61 L. Zhao, W. Lu, M. Ahmed, M. V. Zagidullin, V. N. Azyazov, A. N. Morozov, A. M. Mebel and R. I. Kaiser, Gas-phase synthesis of benzene via the propargyl radical self-reaction, *Sci. Adv.*, 2021, **7**, eabf0360.

62 C. Wentrup and P. Müller, One-step synthesis of fulvene and fulvenallene: thermolysis of Q-coumaranon, phthalide, and benzocyclopropene, *Tetrahedron Lett.*, 1973, **14**, 2915–2918.

63 M. Steinbauer, P. Hemberger, I. Fischer and A. Bodi, Photoionization of C_7H_6 and C_7H_5: observation of the fulvenallenyl radical, *Chemphyschem*, 2011, **12**, 1795–1797.

64 H. W. Jochims, H. Rasekh, E. Rühl, H. Baumgärtel and S. Leach, The photofragmentation of naphthalene and azulene monocations in the energy range 7-22 eV, *Chem. Phys.*, 1992, **168**, 159–184.

65 H. Jin, J. Yang and A. Farooq, Determination of absolute photoionization cross-sections of some aromatic hydrocarbons, *Rapid Commun. Mass Spectrom.*, 2020, **34**, e8899.

66 L. Zhao, R. I. Kaiser, B. Xu, U. Ablikim, M. Ahmed, M. V. Zagidullin, V. N. Azyazov, A. H. Howlader, S. F. Wnuk and A. M. Mebel, VUV photoionization study of the formation of the simplest polycyclic aromatic hydrocarbon: naphthalene ($C_{10}H_8$), *J. Phys. Chem. Lett.*, 2018, **9**, 2620–2626.

67 V. V. Kislov and A. M. Mebel, The formation of naphthalene, azulene, and fulvalene from cyclic C_5 species in combustion: an Ab Initio/RRKM study of 9-H-Fulvalenyl (C_5H_5-C_5H_4) radical rearrangements, *J. Phys. Chem. A*, 2007, **111**, 9532–9543.

68 R. W. Alder, S. P. East, J. N. Harvey and M. T. Oakley, The azulene-to-naphthalene rearrangement revisited: a DFT study of intramolecular and radical-promoted mechanisms, *J. Am. Chem. Soc.*, 2003, **125**, 5375–5387.

69 D. G. Streets and J. Berkowitz, Electronic structures of fulvalene and octachlorofulvalene, *Chem. Phys.*, 1977, **23**, 79–85.

70 L. B. Tuli and A. M. Mebel, Formation of phenanthrene via H-assisted isomerization of 2-ethynylbiphenyl produced in the reaction of phenyl with phenylacetylene, *Int. J. Chem. Kinet.*, 2020, **52**, 875–883.

71 A. W. Jasper and N. Hansen, Hydrogen-assisted isomerizations of fulvene to benzene and of larger cyclic aromatic hydrocarbons, *Proc. Combust. Inst.*, 2013, **34**, 279–287.

72 A. M. Mebel, Y. Georgievskii, A. W. Jasper and S. J. Klippenstein, Pressure-dependent rate constants for PAH growth: formation of indene and its conversion to naphthalene, *Faraday Discuss.*, 2016, **195**, 637–670.

73 R. I. Kaiser, L. Zhao, W. Lu, M. Ahmed, M. V. Zagidullin, V. N. Azyazov and A. M. Mebel, Formation of benzene and naphthalene through cyclopentadienyl-mediated radical–radical reactions, *J. Phys. Chem. Lett.*, 2022, **13**, 208–213.

74 P. Horsch, G. Urbasch and K. Weitzel, Analysis of chirality by femtosecond laser ionization mass spectrometry, *Chirality*, 2012, **24**, 684–690.

75 R. I. Kaiser, L. Zhao, W. Lu, M. Ahmed, V. S. Krasnoukhov, V. N. Azyazov and A. M. Mebel, Unconventional excited-state dynamics in the concerted benzyl (C_7H_7) radical self-reaction to anthracene ($C_{14}H_{10}$), *Nat. Commun.*, 2022, **13**, 786.